Chromatin and Transcriptional Response to Loss of TBX1 in Early Differentiation of Mouse Cells

Andrea Cirino[1,2], Ilaria Aurigemma[1,3], Monica Franzese[4], Gabriella Lania[2], Dario Righelli[3], Rosa Ferrentino[2], Elizabeth Illingworth[3], Claudia Angelini[4]* and Antonio Baldini[1,2]*

[1] Department of Molecular Medicine and Medical Biotechnologies, University of Naples Federico II, Naples, Italy, [2] Institute of Genetics and Biophysics, National Research Council, Naples, Italy, [3] Department of Chemistry and Biology, University of Salerno, Fisciano, Italy, [4] Institute Applicazioni del Calcolo, National Research Council, Naples, Italy

The T-box transcription factor TBX1 has critical roles in the cardiopharyngeal lineage and the gene is haploinsufficient in DiGeorge syndrome, a typical developmental anomaly of the pharyngeal apparatus. Despite almost two decades of research, if and how TBX1 function triggers chromatin remodeling is not known. Here, we explored genome-wide gene expression and chromatin remodeling in two independent cellular models of *Tbx1* loss of function, mouse embryonic carcinoma cells P19Cl6, and mouse embryonic stem cells (mESCs). The results of our study revealed that the loss or knockdown of TBX1 caused extensive transcriptional changes, some of which were cell type-specific, some were in common between the two models. However, unexpectedly we observed only limited chromatin changes in both systems. In P19Cl6 cells, differentially accessible regions (DARs) were not enriched in T-BOX binding motifs; in contrast, in mESCs, 34% ($n = 47$) of all DARs included a T-BOX binding motif and almost all of them gained accessibility in $Tbx1^{-/-}$ cells. In conclusion, despite a clear transcriptional response of our cell models to loss of TBX1 in early cell differentiation, chromatin changes were relatively modest.

Keywords: TBX1, chromatin accessibility, transcriptional response, DiGeorge syndrome, embryonic stell cell

INTRODUCTION

TBX1 is a transcription factor encoded by a gene that is haploinsufficient in DiGeorge/22q11.2 deletion syndromes and in the mouse (Greulich et al., 2011; McDonald-McGinn et al., 2015; Baldini et al., 2017). It is a critical player in the development of the pharyngeal apparatus, which gives rise to organs and structures that are affected by many birth defects. The mechanisms by which TBX1 regulates transcription are only now beginning to emerge, but many questions remain. It binds DNA to a typical T-BOX consensus motif (Castellanos et al., 2014; Fulcoli et al., 2016), and interacts with transcription regulators such as chromatin remodeling complexes, histone modifiers, as well as repressive co-factors (Stoller et al., 2010; Okubo et al., 2011; Chen et al., 2012; Fulcoli et al., 2016), and positively regulates H3K4 monomethylation (Fulcoli et al., 2016). In the mouse, *Tbx1* is expressed early in development (from around E7.5) in the cardiopharyngeal mesoderm, the

developing anterior foregut/pharyngeal endoderm and in the surface ectoderm. Timed-deletion of the gene has revealed a requirement as early as E7.5–E8.0 (Xu et al., 2005) for the development of the 4th pharyngeal arch artery that will form much later. While this phenomenon could be explained by a number of mechanisms, one possibility is that TBX1 primes enhancers for downstream activation or repression, thereby creating asynchrony between the time of requirement and the phenotypic consequences. To address this issue, we have used two cellular models that respond transcriptionally to *Tbx1* gene dosage, mouse P19Cl6 and embryonic stem cells (mESCs), but that are at an early stage of differentiation, and we tested the effects of *Tbx1* inactivation on transcription and on chromatin remodeling. mESCs ($Tbx1^{+/+}$ and $Tbx1^{-/-}$) were subjected to a widely used cardiac mesoderm differentiation protocol (Kattman et al., 2011) and selected using a fluorescence activated cell sorting (FACS) approach. We selected a subpopulation that expresses the highest level of *Tbx1* and pursued it for ATAC-seq (Buenrostro et al., 2015) and RNA-seq. The results obtained from the two cellular models indicate that TBX1 inactivation does not have a strong effect on chromatin remodeling at the differentiation stages tested despite having significant effects on transcription. We discuss possible mechanisms to explain our results.

MATERIALS AND METHODS

P19Cl6 Cells

We plated 5×10^5 cells in a 35-mm dish in Dulbecco-Modified Minimal Essential Medium supplemented (Sigma-Aldrich #M4526) with 10% fetal bovine serum (Gibco #10270106). After 24 h, at confluence, we added 10 uM 5-Azacytidine (5-Aza, Sigma-Aldrich #A2385) to induce differentiation. For ATAC-seq, cells were harvested after a further 24 h. For quantitative ATAC experiments in time course, 24 h after 5-Aza treatment we replaced the media with fresh media containing 1% DMSO. Samples for qATAC were harvested 13 h after transfection (T1), 24 h after 5-Aza induction (D1), and 24 h after DMSO treatment (D2).

Mouse Embryonic Stem Cells (mESCs)

E14-Tg2a mESCs were cultured without feeders and maintained undifferentiated on gelatin-coated dishes in GMEM (Sigma Cat# G5154) supplemented with 10^3 U/ml ESGRO LIF (Millipore, Cat# ESG1107), 15% fetal bovine serum (ES Screened Fetal Bovine Serum, US Euroclone Cat# CHA30070L), 0.1 mM non-essential amino acids (Gibco, Cat# 11140-035), 0.1 mM 2-mercaptoethanol (Gibco, Cat# 31350-010), 0.1 mM L-glutamine (Gibco, Cat# 25030081), 0.1 mM Penicillin/Streptomycin (Gibco, Cat# 10378016), and 0.1 mM sodium pyruvate (Gibco, Cat# 11360-070). The cells were passaged every 2–3 days using 0.25% Trypsin-EDTA (1X) (Gibco, Cat# 25200056) as the dissociation buffer.

For differentiation, E14-Tg2a mESCs were dissociated with Trypsin-EDTA and cultured at 75,000 cells/ml in serum-free media: 75% Iscove's modified Dulbecco's media (Cellgro Cat# 15-016-CV) and 25% HAM F12 media (Cellgro #10-080-CV),

supplemented with N2 (GIBCO #17502048) and B27 (GIBCO #12587010) supplements, penicillin/streptomycin (GIBCO #10378016), 0.05% BSA (Invitrogen Cat#. P2489), L-glutamine (GIBCO #25030081), 5 mg/ml ascorbic acid (Sigma A4544) and 4.5×10^{-4} M monothioglycerol (Sigma M-6145). After 48 h in culture, the EBs were dissociated with trypsin-EDTA and reaggregated for 40 h in serum-free differentiation media with the addition of 8 ng/ml human activin A (R&D Systems Cat#. 338-AC), 0.5 ng/ml human BMP4 (R&D Systems Cat# 314-BP), and 5 ng/ml human VEGF (R&D Systems Cat#. 293-VE). The 2-day-old EBs were dissociated and 6×10^4 cells were seeded onto individual wells of a 24-well plate coated with 0.1% gelatin in StemPro-34 medium (Gibco #10639011), supplemented with SP34 supplement, L-glutamine, 5 mg/ml ascorbic acid, 5 ng/ml human-VEGF, 10 ng/ml human bFGF (R&D Systems 233-FB-025), and 50 ng/ml human FGF10 (R&D Systems 338-FG-025). After 48 h, we added new StemPro-34 media, supplemented with SP34 supplement, L-glutamine, 5 mg/ml ascorbic acid and kept for 96 h. We harvested cells for RNA-seq and ATAC-seq analysis at day 4 of differentiation (**Figure 1A**).

CRISPR-Cas9-Mediated Targeting of mESCs

Tbx1 knockout was induced in E14-Tg2a using Alt-R^{TM} CRISPR-Cas9 System (IDT) following the manufacturer's specifications. This genome editing system is based on the use of a ribonucleoprotein (RNP) consisting of Alt-R S.p. Cas9 nuclease complexed with an Alt-R CRISPR-Cas9 guide RNA (crRNA:tracrRNA duplex). The crRNA is a custom synthesized sequence that is specific for the target (Tbx1KO:/AltR1/rUrG rGrCrC rGrArG rUrArC rArCrU rArCrC rArCrC rGrUrU rUrUrA rGrArG rCrUrA rUrGrC rU/AltR2/) and contains a 16 nt sequence that is complementary to the tracrRNA. Alt-R CRISPR-Cas9 tracrRNA-ATTO 550 (5 nmol catalog no. 1075927) is a conserved 67 nt RNA sequence that is required for complexing to the crRNA so as to form the guide RNA that is recognized by S.p. Cas9 (Alt-R S.p. Cas9 Nuclease 3NLS, 100 μg catalog no. 1081058). The fluorescently labeled tracrRNA with ATTO^{TM} 550 fluorescent dye is used to FACS-purify transfected cells. The protocol involves three steps: (1) annealing of the crRNA and tracrRNA, (2) assembly of the Cas9 protein with the annealed crRNA and tracrRNAs, and (3) delivery of the ribonucleoprotein (RNP) complex into mESC by reverse transfection. Briefly, we annealed equimolar amounts of resuspended crRNA and tracrRNA to a final concentration (duplex) of 1 μM by heating at 95°C for 5 min and then cooling to room temperature. The RNA duplexes were then complexed with Alt-R S.p. Cas9 enzyme in OptiMEM media to form the RNP complex, which was then transfected into mESCs using the RNAiMAX transfection reagent (Invitrogen). After 48 h incubation, cells were trypsinized and ATTO 550 + (transfected) cells were purified by FACS. Fluorescent cells (approximately 65% of the total cell population) were plated at very low density to facilitate colony picking. We picked and screened by PCR 96 clones. Positive clones were confirmed by DNA sequencing.
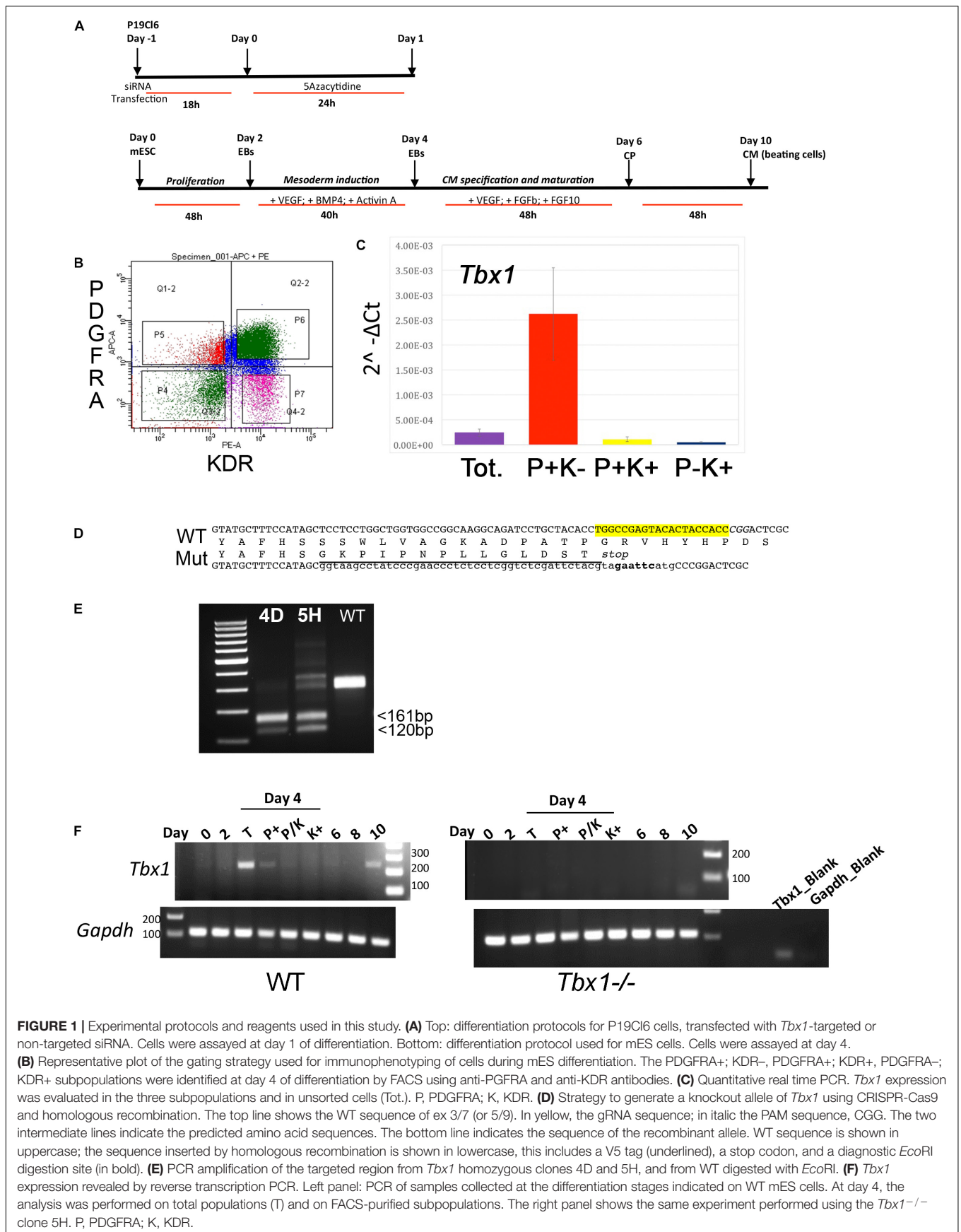
FIGURE 1 | Experimental protocols and reagents used in this study. **(A)** Top: differentiation protocols for P19Cl6 cells, transfected with *Tbx1*-targeted or non-targeted siRNA. Cells were assayed at day 1 of differentiation. Bottom: differentiation protocol used for mES cells. Cells were assayed at day 4.
(B) Representative plot of the gating strategy used for immunophenotyping of cells during mES differentiation. The PDGFRA+; KDR–, PDGFRA+; KDR+, PDGFRA–; KDR+ subpopulations were identified at day 4 of differentiation by FACS using anti-PGFRA and anti-KDR antibodies. **(C)** Quantitative real time PCR. *Tbx1* expression was evaluated in the three subpopulations and in unsorted cells (Tot.). P, PDGFRA; K, KDR. **(D)** Strategy to generate a knockout allele of *Tbx1* using CRISPR-Cas9 and homologous recombination. The top line shows the WT sequence of ex 3/7 (or 5/9). In yellow, the gRNA sequence; in italic the PAM sequence, CGG. The two intermediate lines indicate the predicted amino acid sequences. The bottom line indicates the sequence of the recombinant allele. WT sequence is shown in uppercase; the sequence inserted by homologous recombination is shown in lowercase, this includes a V5 tag (underlined), a stop codon, and a diagnostic *Eco*RI digestion site (in bold). **(E)** PCR amplification of the targeted region from *Tbx1* homozygous clones 4D and 5H, and from WT digested with *Eco*RI. **(F)** *Tbx1* expression revealed by reverse transcription PCR. Left panel: PCR of samples collected at the differentiation stages indicated on WT mES cells. At day 4, the analysis was performed on total populations (T) and on FACS-purified subpopulations. The right panel shows the same experiment performed using the *Tbx1*⁻/⁻ clone 5H. P, PDGFRA; K, KDR.

Fluorescence Activated Cell Sorting (FACS)

For FACS, EBs were collected and allowed to settle by gravity. After washing with PBS, the cells were dissociated using the Embryoid Body dissociation kit (cod. 130-096-348 Miltenyi Biotec) according to the manufacturer's protocol. Dissociated cells (1×10^6 cells/100 μl) were incubated with primary antibodies (PDGFRα-APC, mouse cod.130-102-473; KDR VEGFR2-PE (KDR), mouse cod. 130-120-813 Miltenyi Biotec) directly conjugated (1:50) in PBS-BE solution (PBS, 0.5%BSA, 5 mM EDTA) for 20 min on ice. Subsequently, cells were washed twice with 2 ml of PBS-BE. Cells were sorted using the BD FACS ARIAIII™ cell sorter.

Total RNA was isolated using QIAzol lysis reagent (QIAGEN) and for qRT-PCR it was reverse-transcribed using the High Capacity cDNA Reverse Transcription kit (Applied Biosystem catalog no. 4368814). Quantitative real-time PCR was performed using SYBR Green PCR master mix (Applied Biosystem catalog no. 4309155). Relative gene expression was evaluated using the $2^{-\Delta CT}$ method, and *Gapdh* expression as the normalizer. Primer sequences are listed on **Table 1**.

ATAC-seq Assay

Differentiated P19Cl6 cells and mESCs were collected and then washed two times in PBS, harvested, counted using a hemacytometer chamber and pelleted. 50.000 cells/sample for P19Cl6 and 15.000 cells/sample for mESC were treated with Tagment DNA Buffer 2x reaction buffer with Tagment DNA Enzyme (Illumina) according to the manufacturer's protocol. After washes in PBS, cells were suspended in 50 μL of cold lysis buffer (10 mM Tris-HCl, pH 7.4, 10 mM NaCl, 3 mM MgCl$_2$, 0.1% IGEPAL CA-630) and immediately spun down at $500 \times g$ for 10 min at 4°C. Fresh nuclei were treated with Transposition mix and Purification (Illumina #FC121-130), the nuclei were incubated at 37°C in Transposition Reaction Mix (25 μL reaction buffer, 2.5 μL Transposase, 22.5 μL Nuclease free water), purified using Qiagen MinElute PCR Purification Kit (catalog no./ID: 28006) and eluted in 10 μL of nuclease free water. Sequencing libraries were prepared from linearly amplified tagmented DNA. Fragmentation size was evaluated using the Agilent 4200 TapeStation. We sequenced two biological replicates for each experimental point. Sequencing was performed with an Illumina NextSeq500 machine, in paired-end, 60 bp reads.

Quantitative PCR ATAC (qATAC)

P19Cl6 cells were plated at a density of 5×10^5 cells per well on a 35-mm tissue culture dish containing 25 pmol of a pool of Silencer Select Pre-Designed *Tbx1* siRNA (Life Technology), non-targeted control (Life Technology) and 7.5 μl of RNAiMAX Reagent (Life Technology) diluted in 500 μl of Opti-MEM Medium (Thermo Fischer #31985062). We collected samples at three time points (see P19Cl6 paragraph above and scheme on **Figure 4A**). For each time point we assayed two biological replicates. Cells were collected, washed, trypsinized and counted. Chromatin from 5×10^4 cells was then tagmented, purified

TABLE 1 | Primer sequences.

Gene or locus	Primer sequence
Tbx1 (65 bp)	FW (65 bp): CTGACCAATAACCTGCTGGATGA RV (65 bp): GGCTGATATCTGTGCATGGAGTT
Tbx1 (239 bp)	FW (239 bp): TTTGTGCCCGTAGATGACAA RV (239 bp): AATCGGGGCTGATATCTGTG
Pecam1	FW: TGGTTGTCATTGGAGTGGTC RV: TTCTCGCTGTTGGAGTTCAG
Unc5b	FW: CAATCCAGCCCCACTCAAT RV: GTCCACGCTCCATCCACT
Nanog	FW: AAGTACCTCAGCCTCCAGCA RV: GTGCTGAGCCCTTCTGAATC
Pou5f1	FW: TCAGCTTGGGCTAGAGAAGG RV: TGACGGGAACAGAGGGAAAG
Nrp1	FW: CAGTGGCACAGGTGATGACT RV: TCTGATTGGATGGTGCTGTC
Gapdh	FW: TGCACCACCAACTGCTTAGC RV: TCTTCTGGGTGGCAGTGATG
Bai2	FW: GCAATGACCTGTTCACCACC RV: GCCTGTCTGCGCCATGTATAG
Cdc42bpg	FW: GTAACGTGGCGCAGTTTCTG RV: CCCTCTGCCAATCACCTTCA
Brd4	FW: TCCTCTGAGTCGGAGAGCAC RV: TCCCAGTGTGCCCCTTCTTT
Axin2	FW: TCCGGCTATGTCTTTGCACC RV: TACTCCCCATGCGGTAAGGA
Pxn	FW: GGAGAGATGAGCAGTCCGCA RV: CCATCCACTCTCTGTTCCAGG
Dusp7	FW: CCTCCAAGGTGGTTTCAACA RV: GACGAGCTGTCCACGTTAGT
Positive Control Gapdh-P (Q-ATAC)	FW: GGGAAGCAGCATTCAGGTCT RV: TGAAATGTGCACGCACCAAG
Negative Control (Q-ATAC)	FW: TGCACAACACTGGGCCATTA RV: GTGAGTGAAGGCCATCGGTT
Bai2 (Q-ATAC)	FW: CCAGAGCACTTGCTGTCTGA RV: ACAGTAAGAGGGGACAGGCT
Cdc42bpg (Q-ATAC)	FW: TCAGTCAGCACTGGAAGCTG RV: TCGGAAGGAACTCCACTCCA
Brd4 (Q-ATAC)	FW: TGGGTAGGACGTCACAAACG RV: TCTGCGCCAAATGTCTGACT
Axin2 (Q-ATAC)	FW: CACACCCTCAGAGAACCCAC RV: CAGACTATGGCGGCTTTCCA
Pxn (Q-ATAC)	FW: GCTGCTGCTTCTGCTTCATC RV: GTGGGTCCTCATTGGTCTGG
Dusp7 (Q-ATAC)	FW: CCAGATCCTGCCCTACCTCT RV: GGGTGTGACGTTGAGGATGT
gRNA	TGGCCGAGTACACTACCACC
Oligo for homologous recombination	GAGGTCTTCTGGTTTACCCTATATT GTATGACCCCCCCTCCCACGATG TTGCCCTAGGTATGCTTTCCATAGC GGTAAGCCTATCCCTAACCCTCTCCT CGGTCTCGATTCTACGTAGAATTCAT GCCCGGACTCGCCGGCTAAGGGCGC ACAGTGGATGAAACAGATTGTGTCT TTCGACAAGCTGAAACTGACCAATA

and used for quantitative PCR evaluation. To this end, we have used loci bound by TBX1 (Fulcoli et al., 2016) and located in open chromatin. For real-time PCR, we used biological duplicates for each time point and each duplicate was divided into two

technical replicates. Two different controls were used: *Gapdh* promoter (positive control) representing open chromatin, and a desert island locus (negative control), which does not contain any genes in a range of about 80 kb. Quantification was performed using $2^{-\Delta CT}$ calculation relative to *Gapdh* promoter (positive control). The data are expressed as the average of two biological replicates and the standard deviation. Primer sequences are reported on **Table 1**.

RNA was also extracted from each sample and the expression of genes associated with the above loci was evaluated using real-time reverse transcription PCR (qRT-PCR). Quantitation was performed using relative quantification (RQ) and calculated with the standard error of the mean of two biological replicates.

RNA-seq

mESCs in dishes were washed with cold PBS to which 1 mL of Trizol was added. Lysates were harvested and vortexed in order to promote the lysis of cells. 200 µL of chloroform was added to 1 mL of lyste in order to separate the phases. The mixture was centrifuged at 12000 *g* for 15 min. The upper phase was removed and transferred into a new tube containing 500 µL of isopropanol and the solution was incubated for 20 min at room temperature. After 20 min the solution was centrifuged for 10 min at 12000 *g*. Pelleted RNA was washed twice with Ethanol 80% and centrifuged for 5 min at 7500 *g*. Pellet were resuspended, and the concentration was estimated using a Nanodrop. Libraries were prepared according to the Illumina strand specific RNA-seq protocol. Libraries were sequenced on the Illumina platform NextSeq 500, in paired end, 75 bp reads.

RNA-seq and ATAC-seq Data Analysis

Expressed and differentially expressed (DE) genes related to the analysis of the RNA-seq samples in the P19Cl6 cellular model were retrieved from published datasets (Fulcoli et al., 2016). Mouse ESCs RNA-seq raw sequences were first evaluated for quality using FastQC[1], then mapped to the mouse genome (mm9) using TopHat2 2.0.14 (Kim et al., 2013) with *-r 170 –mate-std-dev 50 –transcriptome-index transcriptome–library-type fr-secondstrand -N 3 –read-edit-dist 5* and all other parameters as default. The transcriptome was built using the Mus_musculus.NCBIM37.67.gtf annotation downloaded from the ensemble database[2]. Only uniquely mappable sequences were retained for further analysis. For each sample, the gene expression was quantified in terms of raw counts using HTseq 0.7.1 (Anders et al., 2015) with *-m intersection-nonempty -s reverse* for all annotated genes. The next analysis was carried out using RNASeqGUI 1.2.1 (Russo et al., 2016), where the expressed genes were first selected using the proportion test, then the raw counts were normalized using the upper quartile method. Finally, the DESeq2 module was used to identify differentially expressed (DE) genes. Genes with adjusted *p*-values < 0.05 were considered DE. Pathway analysis was carried out for both cellular models using gprofiler2 (Raudvere et al., 2019), with the expressed genes as background and a threshold of 0.05 for the FDR value.

For ATAC-seq analysis, FastQC quality check showed 10–20% contamination of Nextera Transposase Sequence primers (Turner, 2014) in the range 33 to 47 bp. We removed these sequences using cutadapt (Martin, 2011) with the following option -a CTGTCTCTTATACACATCTCCGAGCCCACGAGAC -A CTGTCTCTTATACACATCTGACGCTGCCGACGA. Sequences were then aligned to the mouse genome (mm9) using Bowtie2 2.3.4.3 (Langmead and Salzberg, 2012) with the default parameters. Only uniquely mappable reads were retained. A customized R script was used to remove reads with mates mapping to different chromosomes, or with discordant pairs orientation, or with a mate-pair distance > 2 kb, or PCR duplicates (defined as when both mates are aligned to the same genomic coordinate). Reads mapping to the mitochondrial genome were also removed. Coverage heat-maps and average enrichment profiles (TSS ± 10 kb) in each experimental condition were obtained using ngs.plot (Shen et al., 2014) and evaluated on the expressed genes of the cellular models.

ATAC peaks were identified using MACS2 2.1.2.1 (Feng et al., 2012) with the option *–nomodel –shif100 –extsize 200* that are the suggested parameters to handle the Tn5 transposase cut site. In particular, peak calling was performed independently on each ATAC-seq sample of the P19Cl6 cellular model. Then, for each condition a consensus list of enriched regions was obtained using the intersectBed function from the BedTools 2.29 (Quinlan and Hall, 2010), with the default minimum overlap and retaining only the peak regions common to both replicates. In contrast, for the mouse ES cellular model, due to the lower coverage, the two replicates were first merged into a single signal, after which MACS2 was applied to the pooled samples for each experimental condition.

For the P19Cl6 ATAC cellular model, unless otherwise specified, differentially enriched regions (DARs) were obtained using DEScan2 1.6.0 (Righelli et al., 2018) by loading all of the MACS2 peaks, and performing the peak consensus with the finalRegions function (zThreshold = 1, minCarriers = 2 parameters) and using edgeR with estimateDisp, glmQLFit (robust = TRUE parameter), glmQLFTest, in this order and with the defaults parameters. For the pooled mouse ES samples, the function sicer_df (Zang et al., 2009) was used to identify the DARs, setting 200, 400, 0.00001, 0.0001 as parameters for window size (bp), gap size (bp), and FDR_vs_Input, FDR, respectively.

Peaks, consensus peaks, and DARs were annotated with genes using ChIPseeker 1.22 (Yu et al., 2015) by associating to each peak/region the nearest gene, setting the TSS region [−3000, 3000] and downloading the annotation "may2012.archive.ensembl.org" from Biomart (using the makeTxDbFromBiomart function) and the org.Mm.eg.db database. Finally, the annotated genes were intersected with the DE genes.

For both cellular models, transcription factor binding motifs were obtained using the findMotifsGenome program of the HOMER suite[3].

Volcano plots, pie-charts, and other data reshaping were performed using standard R-scripts.

Overlaps among different regions were identified using the intersectBed function from the BedTools 2.29, with default minimum overlap and reporting each original entry once.

RESULTS

Cell Differentiation Models

P19Cl6 cells were subjected to a differentiation protocol that has been previously described (Mueller et al., 2010) (**Figure 1A**). Cells were transfected with scrambled or *Tbx1*-targeted siRNAs, harvested at day 1 of differentiation and processed for ATAC-seq in two biological replicates.

Mouse ES cells were targeted using CRISPR-Cas9 in order to generate a homozygous *Tbx1* loss of function mutation by inserting multiple stop codons and polyA signals into exon 5 by homologous recombination. We obtained two correctly targeted homozygous mutant clones and selected one of them (5H) for further experiments because it did not express any *Tbx1* mRNA (**Figures 1D,E**). Clone 5H and the parental cell line (WT) were subjected to a differentiation protocol (Kattman et al., 2011) according to the scheme shown in **Figure 1A**. WT cells expressed *Tbx1* at day 4, while no expression was detected in *Tbx1*$^{-/-}$ cells (**Figure 1F**).

To enrich for *Tbx1*-expressing cells, we subdivided the population of mES cells by FACS using the standard markers PDGFRA and KDR (a.k.a. VEGFR2) at day 4 of differentiation (**Figure 1B**). We extracted RNA from sorted populations, KDR+; PDGFRa−, KDR+; PDGFRa+, KDR−; PDGFRa+, and from the total, unsorted population. qRT-PCR showed that by far the highest expression of *Tbx1* was in the KDR−; PDGFRa+ population (**Figure 1C**). The same fractionation was performed on *Tbx1*$^{-/-}$ 5H cells and we found that the quantitative distribution of cells in the fractions was similar (**Supplementary Figures S1, S2**). We selected this subpopulation for further experiments solely on the basis of *Tbx1* gene expression, as we aimed at capturing cells at the earliest time point with robust expression of this gene. Therefore, ATAC-seq and RNA-seq assays were performed using KDR−; PDGFRa+ day 4 cells from the WT and *Tbx1*$^{-/-}$ lines, in two biological replicates.

Chromatin Accessibility Assay

P19Cl6 Cells

Control (scrambled siRNA treated) and *Tbx1* depleted (*Tbx1*^{KD}) cells exhibited a similar distribution and intensity of ATAC-seq signal, which was mostly localized to the promoter region of genes, as expected (**Figures 2A–C**).

We next compared ATAC-seq data with TBX1 ChIP-seq data previously reported for this cell line, and under the same differentiation conditions (Fulcoli et al., 2016). Surprisingly, we found that only 80 ATAC peaks (out of a total of 23759 non-targeted siRNA peaks) overlapped with 72 TBX1 ChIP-seq peaks (3% of the 2388 TBX1 peaks), indicating that most TBX1 binding sites are located in closed chromatin, i.e., ATAC-negative.

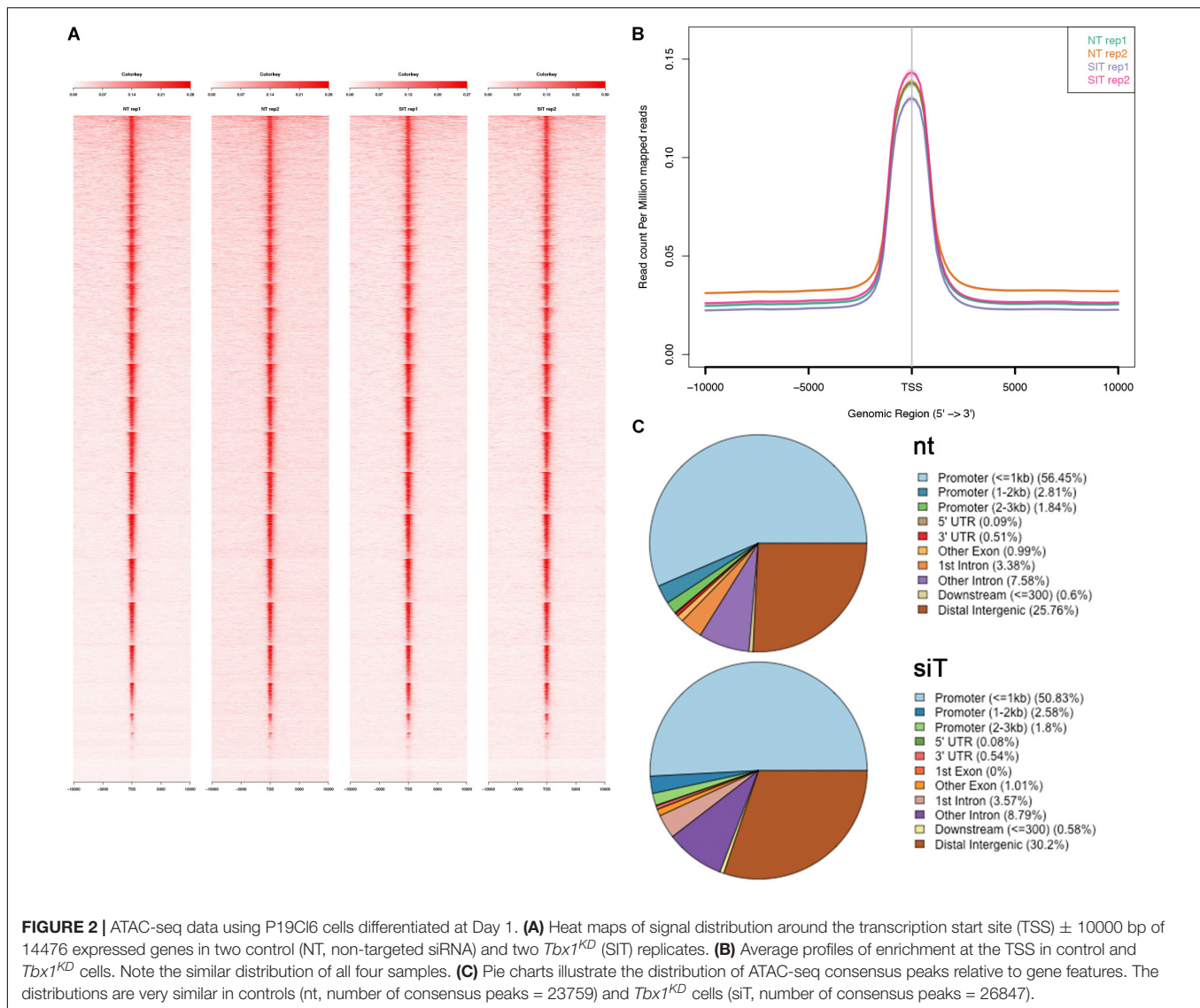We next compared chromatin accessibility profiles in control and *Tbx1*^{KD} cells in order to identify differentially accessible regions (DARs) between the two conditions. We found a total of 177 DARs, of which, 72 (41%) had reduced accessibility and 105 (59%) had increased accessibility following *Tbx1* knockdown (**Figure 3A**). The 177 DARs were annotated with 175 distinct genes, according to Ensembl gene ID (**Supplementary Table S1**). Comparison of this gene list with previously identified differentially expressed genes (DEGs) (Fulcoli et al., 2016) revealed that only 16 (9%) were differentially expressed (**Figure 3A,B**, list in **Supplementary Table S1**); thus, in most cases, chromatin changes identified in our dataset were not associated with transcriptional changes measured by RNA-seq. We examined the distribution of DARs relative to gene features (**Figure 3C**) and found that compared to the distribution of all peaks in the WT population (**Figure 2C**), there was a relatively low presence in the promoter regions (32.2 vs. 61.1%) and a relatively higher representation in distal intergenic regions (42.9 vs. 25.8%).

Analysis of DAR sequences identified a set of known motifs of transcription factors with homeodomains (OCT4, NANOG), high mobility group domains (SOX2, SOX17, SOX15), and zinc finger domains (ZIC1, ZIC2, ZIC3) (**Figure 3D**). Interestingly, several of these proteins are pluripotency factors, but we did not detect any enrichment of T-BOX binding motifs. This is consistent with the finding that only one of all of the DARs identified here overlapped with TBX1 ChIP-seq peaks (indicated in **Supplementary Table S1**).

The finding that almost no TBX1 ChIP-seq peaks changed accessibility after loss of TBX1 was very surprising to us. In order to test whether accessibility changes might follow *Tbx1* KD at a later time than the one tested here, we performed a time-course experiment on 5 ChIP-seq peaks located in open chromatin and associated with five target genes (Fulcoli et al., 2016). The experimental scheme is shown in **Figure 4A**. At each time point, we carried out quantitative ATAC (qATAC) in control and *Tbx1*^{KD} cells. At each point, we also measured the expression of the target genes. The results (**Figures 4B,C**), which were normalized for the accessibility at the GAPDH promoter, confirmed that at D1 (the time tested by ATAC-seq) there was no change in chromatin accessibility. However, at D2, 4 out of 5 loci showed increased accessibility in the *Tbx1*^{KD} condition. In all cases, gene expression changed at earlier time points (T1 or D1, **Figure 4C**), suggesting that differential expression, for these genes, preceded chromatin changes. These results suggest that the effects of *Tbx1* KD on chromatin accessibility are most likely to be indirect.

Mouse ES Cells

We performed ATAC-seq assays on two biological replicates of differentiating WT and *Tbx1*$^{-/-}$ mES cells selected by FACS (PDGFRA+; KDR−). The distribution of ATAC-seq peaks was similar between control and mutant cells (**Figures 5A–C**). We found a total of 138 DARs, of which 26 (19%) decreased accessibility, and 112 (81%) increased accessibility in *Tbx1*$^{-/-}$ cells. Their distribution, compared to WT peaks distribution (**Figure 5C**) showed a relatively lower representation in the promoter regions (43.5 vs. 75.2%) and relatively higher representation in the distal intergenic regions (31.2 vs. 15%),

FIGURE 2 | ATAC-seq data using P19Cl6 cells differentiated at Day 1. **(A)** Heat maps of signal distribution around the transcription start site (TSS) ± 10000 bp of 14476 expressed genes in two control (NT, non-targeted siRNA) and two *Tbx1*^{KD} (SIT) replicates. **(B)** Average profiles of enrichment at the TSS in control and *Tbx1*^{KD} cells. Note the similar distribution of all four samples. **(C)** Pie charts illustrate the distribution of ATAC-seq consensus peaks relative to gene features. The distributions are very similar in controls (nt, number of consensus peaks = 23759) and *Tbx1*^{KD} cells (siT, number of consensus peaks = 26847).
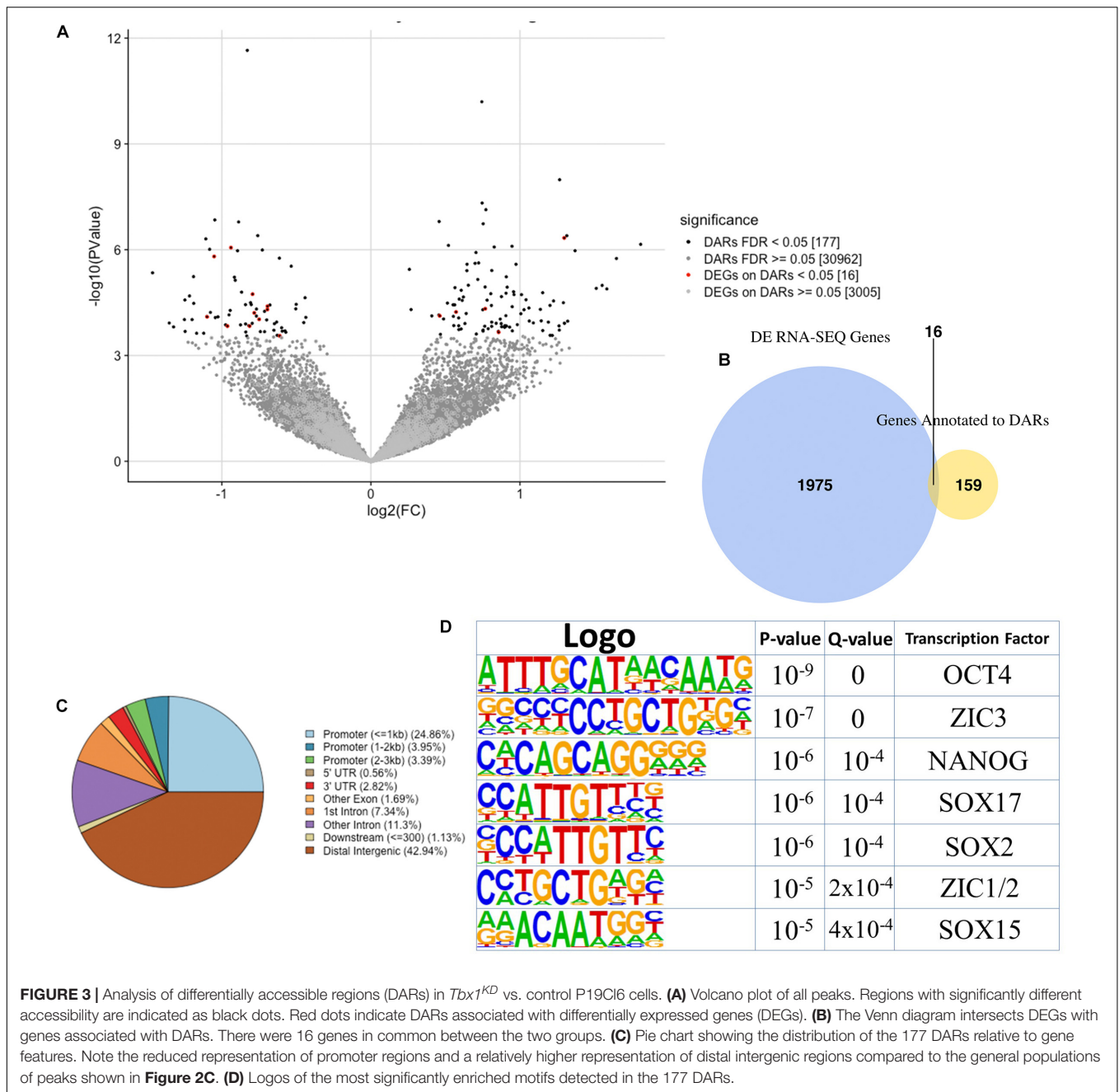
similarly to what we found in P19Cl6 DARs. The 138 peaks were annotated with 138 distinct genes, according to Ensembl gene ID (**Figure 5D** and **Supplementary Table S3**), of which 9 (6.8%) were also differentially expressed (**Supplementary Table S3**). Sequence analysis of DARs revealed an enrichment of T-BOX binding motifs (**Figure 5E**), suggesting that T-BOX proteins, including TBX1 might occupy some of these sites. The two T-BOX motifs shown in **Figure 5E** are almost identical, and one or the other was found in 47 DARs (34% of all DARs) (**Supplementary Table S3**, T-BOX column). Interestingly, 43 out of 47 (91%) were more accessible in mutant cells, suggesting that in these cells, TBX1 may work to maintain the chromatin closed at selected loci, consistent with results obtained in the time course experiment with P19Cl6 cells.

Transcriptional Profiling

Transcriptional changes in response to *Tbx1* knockdown have been reported for P19Cl6 cells (Fulcoli et al., 2016). Here, we

performed RNA-seq analysis on WT and *Tbx1*$^{-/-}$ cells that derive from the same differentiation experiments (two biological replicates) as the ATAC-seq experiments described above. Results revealed 642 genes to be differentially expressed; 412 down-regulated, 230 up regulated in *Tbx1*$^{-/-}$ cell line compared to the parental WT cell line in two biological replicates (**Supplementary Table S2**). We tested the expression of 5 of these differentially expressed genes by qRT-PCR in the total unsorted population, in FACS-purified PDGFRA+; KDR−, PDGFRA+; KDR+, and PDGFRA−; KDR+ cells at day 4 of differentiation. For each population, we tested WT and *Tbx1*$^{-/-}$ genotypes. Results show that differential expression is evident only in the PDGFRA+; KDR− population, indicating that the expression changes are unlikely to be due to generic (non *Tbx1*-linked) differences between cell lines (**Supplementary Figure S3**). A list of all genes expressed in these cells is shown in **Supplementary Table S4**. Next, we carried out functional profiling/gene ontology analyses with g:Profiler2 using DEGs from mES cells and from P19Cl6

FIGURE 3 | Analysis of differentially accessible regions (DARs) in *Tbx1^KD* vs. control P19Cl6 cells. **(A)** Volcano plot of all peaks. Regions with significantly different accessibility are indicated as black dots. Red dots indicate DARs associated with differentially expressed genes (DEGs). **(B)** The Venn diagram intersects DEGs with genes associated with DARs. There were 16 genes in common between the two groups. **(C)** Pie chart showing the distribution of the 177 DARs relative to gene features. Note the reduced representation of promoter regions and a relatively higher representation of distal intergenic regions compared to the general populations of peaks shown in **Figure 2C**. **(D)** Logos of the most significantly enriched motifs detected in the 177 DARs.
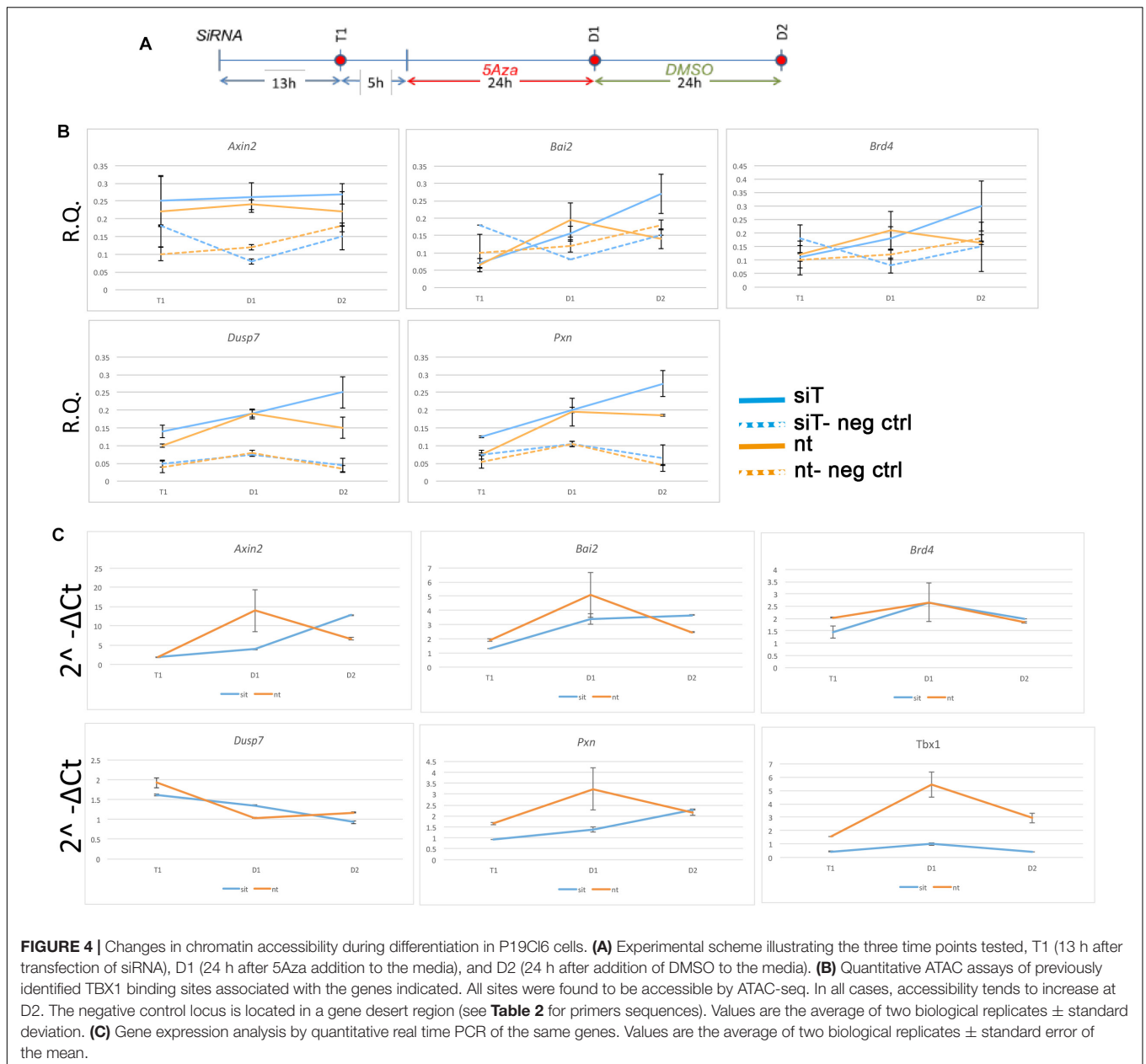
cells (Fulcoli et al., 2016) using identical criteria. Results are shown side-by-side on **Table 2**. Results were very similar in the two models for the gene ontology category "biological process" because in both cases, DEGs were enriched in developmental genes. However, we noted substantial differences in the category of "cellular component" where mESC showed strong enrichment of genes related to the extracellular matrix (ECM), while in contrast, P19Cl6 cells showed enrichment for genes related to intracellular components. KEGG pathway analysis showed again a strong enrichment of ECM-related pathways but with some limited overlap with the P19Cl6 results, as both models showed focal adhesion to be among the enriched pathways. The

enrichment of the KEGG pathways "ECM-receptor interaction" and "basal cell carcinoma" categories in the mESC model is also consistent with recent findings in the mouse (Alfano et al., 2019; Caprio et al., 2020).

DISCUSSION

Data analysis of two cell culture models provided a snapshot of the chromatin accessibility, as measured by ATAC-seq, with and without TBX1 function, or dosage reduction. The use of cell culture systems has limitations because they do not mimic

FIGURE 4 | Changes in chromatin accessibility during differentiation in P19Cl6 cells. **(A)** Experimental scheme illustrating the three time points tested, T1 (13 h after transfection of siRNA), D1 (24 h after 5Aza addition to the media), and D2 (24 h after addition of DMSO to the media). **(B)** Quantitative ATAC assays of previously identified TBX1 binding sites associated with the genes indicated. All sites were found to be accessible by ATAC-seq. In all cases, accessibility tends to increase at D2. The negative control locus is located in a gene desert region (see **Table 2** for primers sequences). Values are the average of two biological replicates ± standard deviation. **(C)** Gene expression analysis by quantitative real time PCR of the same genes. Values are the average of two biological replicates ± standard error of the mean.

complex developmental processes, but they also have some advantages because they are relatively homogeneous compared to whole-organ or whole-embryo material. This is particularly true for our mESC model in which we used a specific subpopulation at a specific differentiation point. In both models, loss of TBX1 led to significant transcriptional changes, as measured by RNA-seq, indicating that both models respond robustly to loss or reduced dosage of TBX1.

In differentiating P19Cl6 cells, the intersection of ATAC signals with a map of TBX1 binding sites, which was previously published for the same cell line and under the same experimental conditions, revealed that almost all of the binding sites were located in ATAC-negative regions. Thus, TBX1 binding does not require accessible chromatin, at least by ATAC assay.

Unfortunately, we were not able to confirm this finding in differentiating mES cells because in our hands, currently available batches of commercial anti-TBX1 antibodies failed to perform in ChIP experiments. In future experiments it will be of interest to establish whether TBX1 can function as a pioneer factor. In a recent paper, it was shown that TBX20, a T-BOX transcription factor that belongs to the same sub-family as TBX1, mostly binds (2/3 of the cases) in closed chromatin regions in endocardial cells (Boogerd et al., 2016). Thus, T-BOX proteins may not need ATAC + regions to bind chromatin. It is also possible that TBX1, at early stages of differentiation, contributes to maintaining the chromatin closed at selected loci. Indeed, in mESC experiments almost all the DARs with a T-BOX binding motif showed increased accessibility in $Tbx1^{-/-}$ cells.
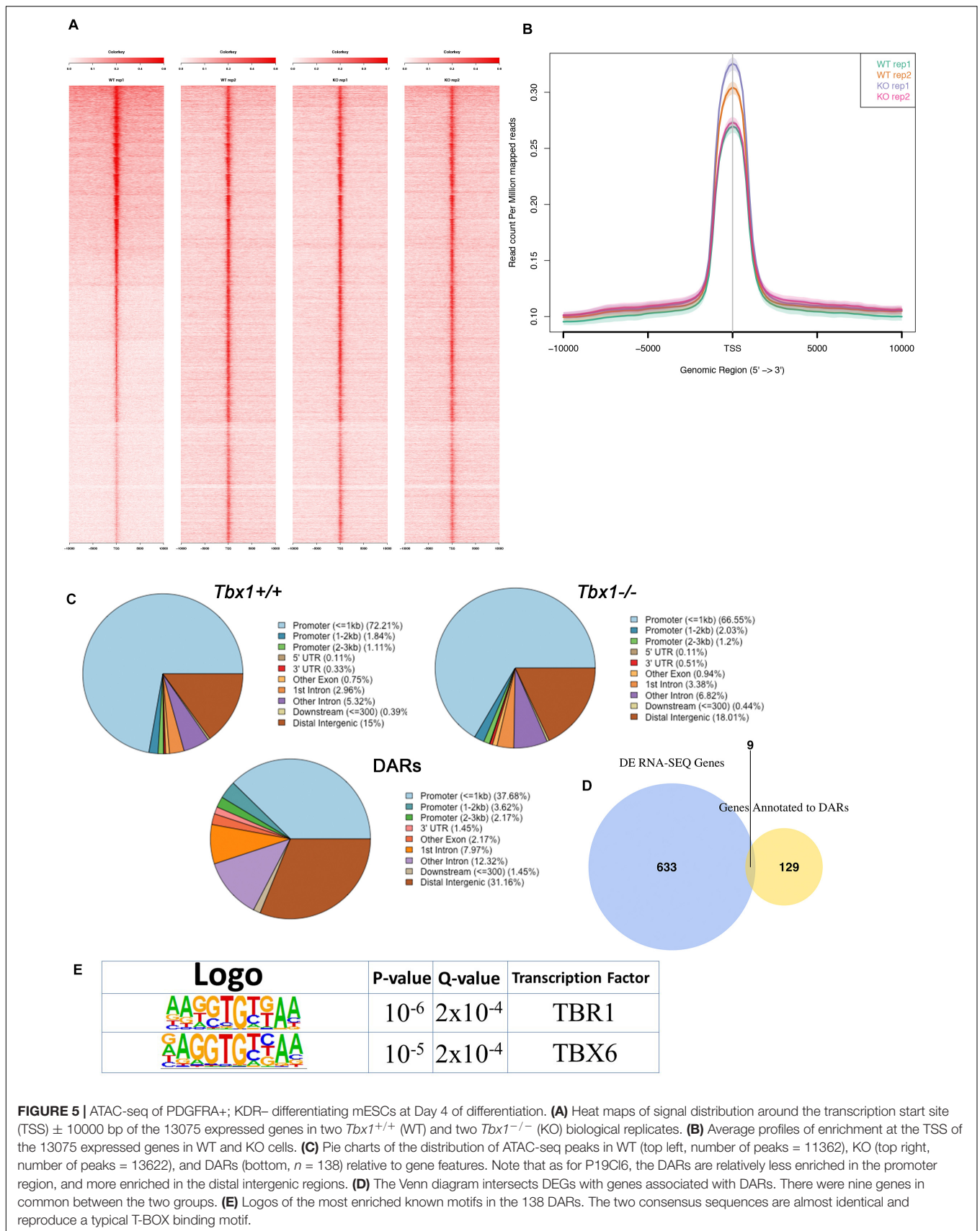
FIGURE 5 | ATAC-seq of PDGFRA+; KDR– differentiating mESCs at Day 4 of differentiation. (A) Heat maps of signal distribution around the transcription start site (TSS) ± 10000 bp of the 13075 expressed genes in two $Tbx1^{+/+}$ (WT) and two $Tbx1^{-/-}$ (KO) biological replicates. (B) Average profiles of enrichment at the TSS of the 13075 expressed genes in WT and KO cells. (C) Pie charts of the distribution of ATAC-seq peaks in WT (top left, number of peaks = 11362), KO (top right, number of peaks = 13622), and DARs (bottom, n = 138) relative to gene features. Note that as for P19Cl6, the DARs are relatively less enriched in the promoter region, and more enriched in the distal intergenic regions. (D) The Venn diagram intersects DEGs with genes associated with DARs. There were nine genes in common between the two groups. (E) Logos of the most enriched known motifs in the 138 DARs. The two consensus sequences are almost identical and reproduce a typical T-BOX binding motif.

TABLE 2 | GO analysis.

	P19Cl6				mESc		
Source	term_id	term_name	p_value	source	term_id	term_name	p_value
Biological process							
GO:BP	GO:0048856	Anatomical structure development	2.66E-08	GO:BP	GO:0007275	Multicellular organism development	4.62E-35
GO:BP	GO:0007275	Multicellular organism development	2.66E-08	GO:BP	GO:0048513	Animal organ development	5.89E-34
GO:BP	GO:0050794	Regulation of cellular process	2.66E-08	GO:BP	GO:0048856	Anatomical structure development	5.89E-34
GO:BP	GO:0032502	Developmental process	5.26E-08	GO:BP	GO:0009653	Anatomical structure morphogenesis	1.08E-33
GO:BP	GO:0048731	System development	7.29E-08	GO:BP	GO:0032502	Developmental process	1.37E-33
GO:BP	GO:0065007	Biological regulation	7.29E-08	GO:BP	GO:0048731	System development	3.80E-33
GO:BP	GO:0050789	Regulation of biological process	7.79E-08	GO:BP	GO:0032501	Multicellular organismal process	9.77E-33
Cellular component							
GO:CC	GO:0005622	Intracellular	2.15E-10	GO:CC	GO:0031012	Extracellular matrix	2.20E-13
GO:CC	GO:0005737	Cytoplasm	9.56E-10	GO:CC	GO:0062023	Collagen-containing extracellular matrix	6.96E-13
GO:CC	GO:0012505	Endomembrane system	4.41E-08	GO:CC	GO:0005576	Extracellular region	2.43E-10
GO:CC	GO:0043229	Intracellular organelle	6.67E-07	GO:CC	GO:0005615	Extracellular space	6.24E-10
GO:CC	GO:0031410	Cytoplasmic vesicle	4.46E-06	GO:CC	GO:0005604	Basement membrane	9.31E-10
GO:CC	GO:0097708	Intracellular vesicle	4.46E-06	GO:CC	GO:0071944	Cell periphery	1.83E-09
GO:CC	GO:0043226	Organelle	4.46E-06	GO:CC	GO:0005886	Plasma membrane	4.45E-09
GO:CC	GO:0031982	Vesicle	6.12E-06	GO:CC	GO:0009986	Cell surface	1.00E-08
GO:CC	GO:0110165	Cellular anatomical entity	6.99E-06	GO:CC	GO:0110165	Cellular anatomical entity	3.50E-06
GO:CC	GO:0005829	Cytosol	1.57E-05	GO:CC	GO:0005587	Collagen type IV trimer	1.68E-05
GO:CC	GO:0048471	Perinuclear region of cytoplasm	0.000242631	GO:CC	GO:0098651	Basement membrane collagen trimer	1.68E-05
Molecular function							
GO:MF	GO:0005515	Protein binding	1.08E-10	GO:MF	GO:0005515	Protein binding	6.12E-10
GO:MF	GO:0019899	Enzyme binding	1.69E-05	GO:MF	GO:0005488	Binding	3.83E-09
GO:MF	GO:0008092	Cytoskeletal protein binding	0.000331085	GO:MF	GO:0005201	Extracellular matrix structural constituent	1.62E-08
GO:MF	GO:0005488	Binding	0.000363156	GO:MF	GO:0008201	Heparin binding	1.58E-07
GO:MF	GO:0071813	Lipoprotein particle binding	0.026237583	GO:MF	GO:0060089	Molecular transducer activity	1.90E-07
GO:MF	GO:0071814	Protein–lipid complex binding	0.026237583	GO:MF	GO:0005102	Signaling receptor binding	3.41E-07
GO:MF	GO:0001067	Regulatory region nuc. acid binding	0.040927289	GO:MF	GO:0005198	Structural molecule activity	3.96E-07
GO:MF	GO:0043168	Anion binding	0.040927289	GO:MF	GO:0005539	Glycosaminoglycan binding	6.98E-07
GO:MF	GO:0016740	Transferase activity	0.040927289	GO:MF	GO:0038023	Signaling receptor activity	6.98E-07
GO:MF	GO:0019900	Kinase binding	0.040927289	GO:MF	GO:0004888	Transmemb. signaling receptor activity	1.04E-06
				GO:MF	GO:0035326	*Cis*-regulatory region binding	2.38E-06
KEGG pathway							
KEGG	KEGG:04810	Regulation of actin cytoskeleton	0.003951158	KEGG	KEGG:04512	ECM-receptor interaction	1.60E-08
KEGG	KEGG:04510	Focal adhesion	0.004660295	KEGG	KEGG:04151	PI3K-Akt signaling pathway	2.72E-06
KEGG	KEGG:04066	HIF-1 signaling pathway	0.004730602	KEGG	KEGG:05165	Human papillomavirus infection	1.00E-05
KEGG	KEGG:05205	Proteoglycans in cancer	0.004730602	KEGG	KEGG:04360	Axon guidance	1.08E-05
KEGG	KEGG:01212	Fatty acid metabolism	0.006364804	KEGG	KEGG:05200	Pathways in cancer	1.08E-05
KEGG	KEGG:00051	Fructose and mannose metabolism	0.008062545	KEGG	KEGG:04390	Hippo signaling pathway	3.33E-05
KEGG	KEGG:05165	Human papillomavirus infection	0.00836325	KEGG	KEGG:05146	Amebiasis	0.000184329
KEGG	KEGG:04140	Autophagy – animal	0.00836325	KEGG	KEGG:05206	MicroRNAs in cancer	0.000205893
KEGG	KEGG:05223	Non-small cell lung cancer	0.00836325	KEGG	KEGG:05205	Proteoglycans in cancer	0.000273917
KEGG	KEGG:04934	Cushing syndrome	0.008904189	KEGG	KEGG:04550	Signaling path. pluripotency of stem cells	0.000328595
KEGG	KEGG:05206	MicroRNAs in cancer	0.010714853	KEGG	KEGG:04350	TGF-beta signaling pathway	0.000402713
KEGG	KEGG:05214	Glioma	0.012951127	KEGG	KEGG:01100	Metabolic pathways	0.000415169
KEGG	KEGG:05163	Human cytomegalovirus infection	0.013108615	KEGG	KEGG:04510	Focal adhesion	0.000454709
KEGG	KEGG:04152	AMPK signaling pathway	0.01346403	KEGG	KEGG:01230	Biosynthesis of amino acids	0.000852464
KEGG	KEGG:05215	Prostate cancer	0.01346403	KEGG	KEGG:05217	Basal cell carcinoma	0.001326581

Gene ontology (GO) analysis of DEGs in response to loss of TBX1 in the two models revealed broad differences, but also some similarities. In both cases, DEGs were enriched in genes involved in developmental processes, as expected; in both cases, the focal adhesion KEGG pathway was significantly enriched. The latter has been

validated recently in different cultured cells and in mouse mutants (Alfano et al., 2019). However, in general, GO enrichment was more dispersed in P19Cl6 cells compared to differentiated mES cells, where there was higher enrichment of specific GO terms, perhaps reflecting a more differentiated state and/or a more homogeneous cell population. Particularly evident was the presence of ECM-related genes in the mESC-derived cells.

We selected PDGFRA+; KDR− cells for our studies on the basis of *Tbx1* gene expression; data in the literature suggest that mESC-derived PDGFRA+; KDR− cells have a marker profile that is similar to paraxial mesoderm (Sakurai et al., 2006; Tanaka et al., 2009; Craft et al., 2013), which includes head mesenchyme, a tissue that expresses high levels of *Tbx1*. The mesenchymal nature of the PDGFRA+; KDR− cell population is also consistent with high expression of genes encoding collagens and vimentin. *Tbx1*-expressing mesenchymal cells contribute to various tissues of the neck and face, including some muscle, bones, and connective tissue (Adachi et al., 2020).

P19Cl6 cells were chosen for our experiments because: (a) availability of a Tbx1 ChIP-seq map; (b) availability of an established protocol to differentiate these cells into a cardiomyocyte lineage; and (c) evidence that loss of *Tbx1* alters transcription. The results presented here, however, suggest that the mESCs may be a better model because of the opportunity to obtain more relevant cell types. Nevertheless, in terms of chromatin remodeling, the overall results were consistent in the two models. Indeed, despite a significant transcriptional response to loss of TBX1, we detected a very modest chromatin response in both models. We cannot exclude that the selected differentiation protocols might have affected the ability of TBX1 to remodel chromatin. For example the use of 5-Aza, a DNA methylation inhibitor, might have created an artificial chromatin landscape in P19Cl6 cells. However, because the use of two different protocols has yielded similar results, we believe that overall our data are not significantly biased by the protocols used.

We have previously proposed that TBX1 is a priming factor that regulates deposition of H3K4me1 in H3K27Ac-negative regions, presumed to be inactive enhancers (Fulcoli et al., 2016). The finding of closed chromatin at TBX1 binding sites is indirectly supported by the findings that in P19Cl6 cells, binding regions generally lack acetylation of H3K27, and that genes associated with TBX1 ChIP-seq peaks showed low level of expression (Fulcoli et al., 2016). However, H3K4me1 triggers a number of mechanisms that eventually lead to the opening of the chromatin (reviewed in Calo and Wysocka, 2013). Thus, we would have expected a more extensive chromatin remodeling than the one that we observed. However, H3K4me1 deposition may also lead to long range chromatin changes, which were not tested in our experiments (Yan et al., 2018). In any case, it is possible that the putative priming activity of TBX1 leads to chromatin changes that are downstream of the differentiation time window tested here. TBX1 has been shown to interact with multiple proteins. Absence or insufficient concentration of critical interactors in the models tested might have reduced the ability of TBX1 to remodel chromatin. The observed late chromatin remodeling in response to loss of

TBX1 (**Figure 4**) suggests that the transcription factor may prime enhancers, which are later bound by other factors that are responsible for remodeling. A recent study tested the effect of FOXA2 loss of function on chromatin remodeling during ES-based endoderm differentiation into pancreatic cells (Lee et al., 2019). FOXA2 is a pioneer transcription factor that, like TBX1, regulates H3K4me1 deposition in early phases of differentiation (to definitive endoderm), but its loss did not cause significant ATAC-seq changes at this stage. It was only at later stages of differentiation, when H3K27 acetylation occurred, that ATAC-seq changes became significant (Lee et al., 2019). Our qATAC time course results, though limited to a small number of loci, is consistent with the hypothesis that chromatin remodeling may occur at later stages of differentiation.

The development of optimized protocols that will allow the monitoring of *Tbx1*-expressing cells throughout their differentiation will help to address this hypothesis in the future.

DATA AVAILABILITY STATEMENT

The datasets generated for this study can be found in NCBI SRA, accession PRJNA641413.

AUTHOR CONTRIBUTIONS

AC, IA, GL, and RF performed wet lab experiments. AC, MF, DR, and CA performed bioinformatics data analysis. EI, CA, and AB provided funds. AB wrote the manuscript. EI, AC, IA, GL, and CA contributed to writing and editing. All authors contributed to the article and approved the submitted version.

FUNDING

ACKNOWLEDGMENTS

SUPPLEMENTARY MATERIAL

The Supplementary Material for this article can be found online at: https://www.frontiersin.org/articles/10.3389/fcell.2020. 571501/full#supplementary-material

FIGURE S1 | Analysis of surface markers PDGFRA and KDR expression in *Tbx1*^{+/+} and *Tbx1*^{−/−} mESC lines at day 4 of differentiation. **(A,D)** *Tbx1*^{+/+} and

$Tbx1^{-/-}$ cells labeled by primary antibodies PDGFRA (APC-A) and KDR (PE-A). 4 fractions were identified: Q1-2 = PDGFRA+/KDR−; Q2-2 = PDGFRA+/KDR+; Q4-2 = PDGFRA−/KDR+; Q3-2 = PDGFRA-/KDR−; **(B,C,E,F)** Negative controls (NC) are cells not incubated with primary antibodies.

FIGURE S2 | Plots showing FACS controls. **(A)** $Tbx1^{+/+}$ cells labeled by PDGFRA-APC antibody and isotype control-PE (left); and by isotype control-APC and KDR-PE antibodies (right); **(B)** $Tbx1^{-/-}$ cells labeled by PDGFRA-APC antibody; and isotype control-PE (left), by isotype control-APC and KDR-PE antibodies (right).

FIGURE S3 | Plots showing gene expression assays of five genes in differentiating mESCs. These genes were identified as differentially expressed by RNA-seq in sorted PDGFRA+; KDR− cells. Quantitative real time PCR in unsorted cells at D4 (WT d4 tot. and $Tbx1^{-/-}$ d4 tot.) and in sorted subpopulations showed that the clearest differential expression is only detected in the PDGFRA+; KDR− subpopulation (data shaded in yellow) for all genes tested.

TABLE S1 | Differentially accessible regions in P19Cl6 cells with gene annotation, intersection with differentially expressed genes, and intersection with TBX1 ChIP-seq peaks.

TABLE S2 | Differentially expressed genes in differentiating mESC. Columns contain the Ensembl Identifier, the corresponding Gene Symbol, the log2 FoldChange of KO/WT and the Adjusted p-value (cut off = 0.05).

TABLE S3 | Differentially accessible regions in differentiating mES cells with gene annotation, intersection with differentially expressed genes.

TABLE S4 | Genes expressed in PDGFRA+; KDR− mES cells at d4. Columns contain the Ensembl Identifier, the corresponding Gene Symbol and the normalized upper quartile gene expression counts for each sample.

REFERENCES

Adachi, N., Bilio, M., Baldini, A., and Kelly, R. G. (2020). Cardiopharyngeal mesoderm origins of musculoskeletal and connective tissues in the mammalian pharynx. *Development* 147:dev185256. doi: 10.1242/dev.185256

Alfano, D., Altomonte, A., Cortes, C., Bilio, M., Kelly, R. G., and Baldini, A. (2019). Tbx1 regulates extracellular matrix-cell interactions in the second heart field. *Hum. Mol. Genet.* 28, 2295–2308. doi: 10.1093/hmg/ddz058

Anders, S., Pyl, P. T., and Huber, W. (2015). HTSeq–a Python framework to work with high-throughput sequencing data. *Bioinforma. Oxf. Engl.* 31, 166–169. doi: 10.1093/bioinformatics/btu638

Baldini, A., Fulcoli, F. G., and Illingworth, E. (2017). Tbx1: transcriptional and developmental functions. *Curr. Top. Dev. Biol.* 122, 223–243.

Boogerd, C. J., Aneas, I., Sakabe, N., Dirschinger, R. J., Cheng, Q. J., Zhou, B., et al. (2016). Probing chromatin landscape reveals roles of endocardial TBX20 in Septation. *J. Clin. Invest.* 126, 3023–3035. doi: 10.1172/jci85350

Buenrostro, J. D., Wu, B., Chang, H. Y., and Greenleaf, W. J. (2015). ATAC-seq: a method for assaying chromatin accessibility genome-wide. *Curr. Protoc. Mol. Biol.* 109, 21.29.1–21.29.9.

Calo, E., and Wysocka, J. (2013). Modification of enhancer chromatin: what, how, and why? *Mol. Cell* 49, 825–837. doi: 10.1016/j.molcel.2013.01.038

Caprio, C., Varricchio, S., Bilio, M., Feo, F., Ferrentino, R., Russo, D., et al. (2020). TBX1 and basal cell carcinoma: expression and Interactions with Gli2 and Dvl2 Signaling. *Int. J. Mol. Sci* 21:607. doi: 10.3390/ijms21020607

Castellanos, R., Xie, Q., Zheng, D., Cvekl, A., and Morrow, B. E. (2014). Mammalian TBX1 preferentially binds and regulates downstream targets via a tandem T-site repeat. *PLoS One* 9:e95151. doi: 10.1371/journal.pone.0095151

Chen, L., Fulcoli, F. G., Ferrentino, R., Martucciello, S., Illingworth, E. A., and Baldini, A. (2012). Transcriptional control in cardiac progenitors: Tbx1 interacts with the BAF chromatin remodeling complex and regulates Wnt5a. *PLoS Genet.* 8:e1002571. doi: 10.1371/journal.pgen.1002571

Cirino, A., Aurigemma, I., Franzese, M., Lania, G., Righelli, D., Ferrentino, R., et al. (2020). Chromatin and transcriptional response to loss of TBX1 in early differentiation of mouse cells. *biorxiv* [Preprint]. doi: 10.1101/2020.06.06.137026

Craft, A. M., Ahmed, N., Rockel, J. S., Baht, G. S., Alman, B. A., Kandel, R. A., et al. (2013). Specification of chondrocytes and cartilage tissues from embryonic stem cells. *Development* 140, 2597–2610. doi: 10.1242/dev.087890

Feng, J., Liu, T., Qin, B., Zhang, Y., and Liu, X. S. (2012). Identifying ChIP-seq enrichment using MACS. *Nat. Protoc.* 7, 1728–1740. doi: 10.1038/nprot.2012.101

Fulcoli, F. G., Franzese, M., Liu, X., Zhang, Z., Angelini, C., and Baldini, A. (2016). Rebalancing gene haploinsufficiency in vivo by targeting chromatin. *Nat. Commun.* 7:11688.

Greulich, F., Rudat, C., and Kispert, A. (2011). Mechanisms of T-box gene function in the developing heart. *Cardiovasc. Res.* 91, 212–222. doi: 10.1093/cvr/cvr112

Kattman, S. J., Witty, A. D., Gagliardi, M., Dubois, N. C., Niapour, M., Hotta, A., et al. (2011). Stage-specific optimization of activin/nodal and BMP signaling promotes cardiac differentiation of mouse and human pluripotent stem cell lines. *Cell Stem Cell* 8, 228–240. doi: 10.1016/j.stem.2010.12.008

Kim, D., Pertea, G., Trapnell, C., Pimentel, H., Kelley, R., and Salzberg, S. L. (2013). TopHat2: accurate alignment of transcriptomes in the presence of insertions, deletions and gene fusions. *Genome Biol.* 14:R36. doi: 10.1186/gb-2013-14-4-r36

Langmead, B., and Salzberg, S. L. (2012). Fast gapped-read alignment with Bowtie 2. *Nat. Methods* 9, 357–359. doi: 10.1038/nmeth.1923

Lee, K., Cho, H., Rickert, R. W., Li, Q. V., Pulecio, J., Leslie, C. S., et al. (2019). FOXA2 Is required for enhancer priming during pancreatic differentiation. *Cell Rep.* 28, 382.e7–393.e7.

Martin, M. (2011). Cutadapt removes adapter sequences from high-throughput sequencing reads. *EMBnet.J.* 17, 10–12. doi: 10.14806/ej.17.1.200

McDonald-McGinn, D. M., Sullivan, K. E., Marino, B., Philip, N., Swillen, A., Vorstman, J. A. S., et al. (2015). 22q11.2 deletion syndrome. *Nat. Rev. Dis. Primer.* 1:15071.

Mueller, I., Kobayashi, R., Nakajima, T., Ishii, M., and Ogawa, K. (2010). Effective and steady differentiation of a clonal derivative of P19CL6 embryonal carcinoma cell line into beating cardiomyocytes. *J. Biomed. Biotechnol.* 2010:380561.

Okubo, T., Kawamura, A., Takahashi, J., Yagi, H., Morishima, M., Matsuoka, R., et al. (2011). Ripply3, a Tbx1 repressor, is required for development of the pharyngeal apparatus and its derivatives in mice. *Development* 138, 339–348. doi: 10.1242/dev.054056

Quinlan, A. R., and Hall, I. M. (2010). BEDTools: a flexible suite of utilities for comparing genomic features. *Bioinforma. Oxf. Engl.* 26, 841–842. doi: 10.1093/bioinformatics/btq033

Raudvere, U., Kolberg, L., Kuzmin, I., Arak, T., Adler, P., Peterson, H., et al. (2019). g:Profiler: a web server for functional enrichment analysis and conversions of gene lists (2019 update). *Nucleic Acids Res.* 47, W191–W198.

Righelli, D., Koberstein, J., Zhang, N., Angelini, C., Peixoto, L., and Risso, D. (2018). Differential enriched Scan 2 (DEScan2): a fast pipeline for broad peak analysis. *PeerJ Inc.* 6:e27357v1.

Russo, F., Righelli, D., and Angelini, C. (2016). Advancements in RNASeqGUI towards a reproducible analysis of RNA-Seq experiments. *BioMed Res. Int.* 2016:7972351.

Sakurai, H., Era, T., Jakt, L. M., Okada, M., Nakai, S., Nishikawa, S., et al. (2006). In vitro modeling of paraxial and lateral mesoderm differentiation reveals early reversibility. *Stem Cells Dayt. Ohio* 24, 575–586. doi: 10.1634/stemcells.2005-0256

Shen, L., Shao, N., Liu, X., and Nestler, E. (2014). ngs.plot: quick mining and visualization of next-generation sequencing data by integrating genomic databases. *BMC Genomics* 15:284. doi: 10.1186/1471-2164-15-284

Stoller, J. Z., Huang, L., Tan, C. C., Huang, F., Zhou, D. D., Yang, J., et al. (2010). Ash2l interacts with Tbx1 and is required during early embryogenesis. *Exp. Biol. Med. Maywood* 235, 569–576. doi: 10.1258/ebm.2010.009318

Tanaka, M., Jokubaitis, V., Wood, C., Wang, Y., Brouard, N., Pera, M., et al. (2009). BMP inhibition stimulates WNT-dependent generation of chondrogenic mesoderm from embryonic stem cells. *Stem Cell Res.* 3, 126–141. doi: 10.1016/j.scr.2009.07.001

Turner, F. S. (2014). Assessment of insert sizes and adapter content in fastq data from NexteraXT libraries. *Front. Genet.* 5:5. doi: 10.3389/fgene.2014.00005

Xu, H., Cerrato, F., and Baldini, A. (2005). Timed mutation and cell-fate mapping reveal reiterated roles of Tbx1 during embryogenesis, and a crucial function during segmentation of the pharyngeal system via regulation of endoderm expansion. *Development* 132, 4387–4395. doi: 10.1242/dev. 02018

Yan, J., Chen, S.-A. A., Local, A., Liu, T., Qiu, Y., Dorighi, K. M., et al. (2018). Histone H3 lysine 4 monomethylation modulates long-range chromatin interactions at enhancers. *Cell Res.* 28, 204–220. doi: 10.1038/cr. 2018.1

Yu, G., Wang, L.-G., and He, Q.-Y. (2015). ChIPseeker: an R/Bioconductor package for ChIP peak annotation, comparison and visualization. *Bioinforma. Oxf. Engl.* 31, 2382–2383. doi: 10.1093/bioinformatics/btv145

Zang, C., Schones, D. E., Zeng, C., Cui, K., Zhao, K., and Peng, W. (2009). A clustering approach for identification of enriched domains from histone modification ChIP-Seq data. *Bioinforma. Oxf. Engl.* 25, 1952–1958. doi: 10. 1093/bioinformatics/btp340